ChemPubSoc Europe

DOI: 10.1002/slct.201601229

Chemistry SELECT Full Papers

Materials Science inc. Nanomaterials & Polymers

# Optoelectronic Properties of Layered Titanate Nanostructure and Polyaniline Impregnated Devices

Sesha Vempati,*[a] Yelda Ertas,[a, b] V. Jagadeesh Babu,*[a] and Tamer Uyar[a, b]

Integrated structure of titanate nanotubes and nanosheets is investigated for their optical, electronic and optoelectronic properties when combined with HCl doped polyaniline (PANI). HR-TEM, SEM and XRD were employed for detailed morphological and microstructural understanding of the orthorhombic titanate nanostructure. Chemisorbed oxygeneous groups are probed with Raman spectroscopy which are found to desorb under UV-Vis treatment. We note a blue shift of Ti-O-Ti Raman frequency in contrast to Na-O-Ti stretching. Valence band region of titanate is analyzed for contribution of O2p, O2s, Na2p and Ti3p. Photoluminescence with different excitation energies revealed the presence of oxygen vacancy related defects in titanate. The highly occupied electronic states of PANI were also analyzed until 40 eV below the Fermi energy. XPS core-level analyses revealed ~25% doping density in PANI. Edges of valence band and HOMO are determined to be at 2.45 eV and 2.54 eV below Fermi energy for titanate and PANI, respectively. ITO/PANI/ITO has depicted negative photoresponse and the magnitude of which is reduced ~4 times after combining with titanate nanostructure. Essentially the nanoscale architecture separates the emeraldine base and salt regions of PANI. This separation channelizes the charge carriers before trapping which reduces the magnitude of the negative photoresponse.

## Introduction

Layered titanates are known for more than 30 years,[1] nevertheless, the research interest on layered nanostructures is prevailing recently.[2] Their interlayer chemical, ion exchange and physical properties enhance their vast application potential in solar cells,[2g] lithium ion batteries,[2h] catalysis,[2i] and others.[2a–c,j] All these applications require a deeper understanding of surface/bulk optoelectronic properties. Although there are a few studies in the literature[3] the optical properties were not elaborately investigated and discussed. Despite these studies hint a distinct photoluminescence (PL) depending on the intrinsic defects and/or dopants.[3b] The complete exploitation of any material is achieved under device configuration, for which a clear understanding of the charge generation and subsequent recombination are essential. In the context of devices, two broad classifications can be realized, *viz* nanocomposites and heterojunctions. Here we have adopted nanocomposite of the layered titanate with a model conducting polymer to study the device proerties. However, interestingly, the nanoscale architecture of titanate is preserved in millimeter scale where a conducting polymer is impregnated within the structure. We have chosen HCl doped polyaniline (PANI), well investigated and potential conducting polymer,[4] especially in the context of photoconductivity.[4a] PANI is not charge conjugation symmetric[4b] however, the electrical conduction takes place via hopping mechanism and depicts a negative photoresponse (PR).[4a] By a systematic characterization and subsequent device fabrication we unravel the PR of the layered titanate device when combined with PANI. It is notable that the titanate materials were not elaborately explored in the context of composite devices.[2g,j,5]

In this report we have investigated the structural and electronic properties of titanate nanostructure of a complex architecture consisting of nanotubes and nano-tubes and -sheets. Apart from morphological and microstructural studies, the presence of chemisorbed oxygeneous groups is probed. In the context of electronic structure, occupied electronic states were investigated for titanate and HCl doped PANI unveiling various molecular orbital contributions. Wavelength dependent PL spectra revealed the presence of oxygen related defects. Titanate and PANI based devices depicted ~4 times reduction in the magnitude of PR and attributed to an effective channelization of the photogenerated charge carriers before trapping.

## Results and Discussion

TEM images from titanate sample are shown in Figure 1a and b which unveil an interesting layered structure. Also see low magnification SEM image as insert of Figure 1a revealing the uniformity of the material. The high resolution micrograph (insert of Figure 1b) evidenced the layers with an interlayer distance of 0.7-0.8 nm which is consistent with literature.[6]

[a] *Dr. S. Vempati, Y. Ertas, Dr. V. J. Babu, Prof. T. Uyar*
UNAM-National Nanotechnology Research Center
Bilkent University
Ankara-06800, Turkey
E-mail: svempati01@qub.ac.uk
vjbabu2002@gmail.com

[b] *Y. Ertas, Prof. T. Uyar*
UNAM-Institute of Materials Science & Nanotechnology
Bilkent Univeristy
Ankara-06800, Turkey

Supporting information for this article is available on the WWW under http://dx.doi.org/10.1002/slct.201601229

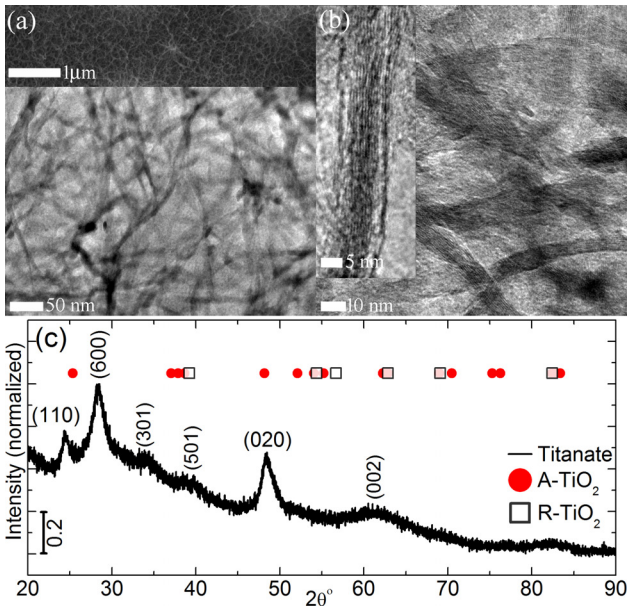


**Figure 1.** (a) and (b) TEM micrographs and (c) XRD pattern from titanate nanostructures. Insert of (a) and (b) are SEM and HR-TEM micrographs, respectively.

Going into the specifics the distance between two adjacent O atoms is 0.3 nm which are located at the topmost corners of the octahedra sharing the edges (zigzag structure). In the process of synthesis $TiO_2$-$SiO_2$-polyvinyl acetate nanofibers were calcined followed by a treatment with NaOH solution.[2g,3a] The alkali treatment etched away the $SiO_2$ and facilitated the structural rearrangement of titanate. The conversion mechanism is believed to contain a number of steps.[2a,7] Morgado et al.[8] explicitly pointed out the discrepancies in determining the actual crystal structure of these layered titanates and extensively discussed the formation dynamics. Initially under NaOH treatment the alkali ion breaks the longer Ti-O-Ti bonds.[9] In the second stage of reaction, Ti-O-Na bonds will be hydrolyzed (partial/complete) with water/HCl forming Ti-O-H. Ti-O-H bond formation is accompanied by the creation of linear fragments, which upon rearrangement transforms into sheets/ribbons of edge sharing octahedra with $Na^+$ and $OH^-$ intercalated between the sheets. The morphology of the final titanate is determined by the initial polymorph of $TiO_2$ (anatase/rutile), nature of the alkali, its concentration and the reaction temperature.[2a,7] In the present context the sheets self-assemble or fold to create tubular nanostructures connected with membranes (refer to the TEM images). This complex though regular architecture enables a very high surface area to volume ratio. Due to scrolling of the lamellar titanate nanosheet lattice distortions/defects can be expected which may host foreign atoms, molecules or ions.[2i]

XRD pattern from titanate nanostructure is shown in Figure 1c. Indices corresponding to various peaks are annotated on the image. Reflections from possible phases of $TiO_2$ such as anatase (A-$TiO_2$) and rutile (R-$TiO_2$) were overlaid on the pattern. It is clear that either of the $TiO_2$ phases were not present within the detection limits of XRD. The analysis of the diffraction pattern yielded the lattice parameters as $a = 18.79$ Å, $b = 3.75$ Å, and $c = 2.85$ Å, where $a$ corresponds to the interlayer distance. These parameters suggest an orthorhombic lattice with the unit cell volume of 199.85 Å$^3$. The distance between the two adjacent layers of the present nanostructure ($a$) is higher than that of layered type (16.66 Å Ref.[10]). The crystallite size based on (600) reflection is calculated to be ~52 Å (for a shape factor of 0.94 and assuming spherical crystals with cubic symmetry).[11] Furthermore, the surface area is ~233 m$^2$/g for two formula units with a molecular weight of 301.62 g/mol.[2g] Overall the titanate sample depicted peaks those are similarly positioned to that of layered titanates such as $H_2Ti_3O_7$, $H_2Ti_2O_5{\cdot}H_2O$, and lepidocrocite titanates.[7e,12] Essentially the present nanostructure is a layered titanate.[7e,12] Previous investigation suggested a predominant $Na_{2-x}H_xTi_2O_4(OH)_2$ phase which is believed to be the case here as well.[2g,3a]

The Raman spectra from titanate nanostructures are shown in Figure 2 comparing two cases with reference to UV-vis

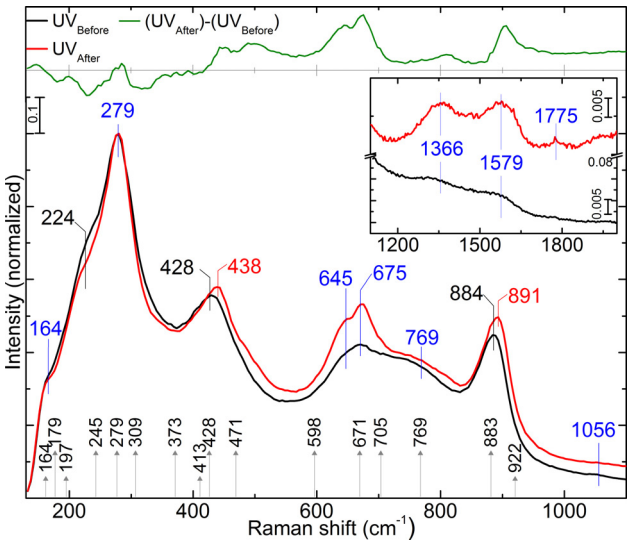


**Figure 2.** Raman spectra from titanate nanostructures before and after UV-Vis treatment. The difference spectrum is also shown.

treatment, *viz* before ($UV_{Before}$) and after ($UV_{After}$) the treatment. Such a comparison would unfold interesting properties which may be connected to the surface related adsorbates. The nanostructure is closely comparable to a *'sponge-like'* structure bearing a significant area that is exposed to ambient. Raman active modes corresponding to A-$TiO_2$ (144, 397, 516, and 640 cm$^{-1}$) or R-$TiO_2$ (144, 250, 446 and 610 cm$^{-1}$) are not observed within the detection limits. The spectra were normalized with reference to the intensity of the strongest band at 279 cm$^{-1}$. It is interesting to note the variations between the spectra, see the difference spectrum ($UV_{After} - UV_{Before}$) within 130–1100 cm$^{-1}$ range. Various Raman bands from the literature[13] are annotated on the image. Firstly, we discuss the $UV_{Before}$ spectrum. The analysis of XRD pattern

revealed orthorhombic crystal structure, along with a predominant $Na_{2-x}H_xTi_2O_4(OH)_2$ phase.[2g] Interestingly, the Raman spectral features from the $Na_{2-x}H_xTi_2O_4(OH)_2$ are similar to that of $Na_2Ti_3O_7$,[14] apart from the differences in the relative intensities of the vibrational bands. The intensity differences were attributed to microstructure of the titanate, see for instance, Ref.[13] where continuous and nearly parallel nanorods were investigated. Explicit bands were observed at ~164, 224, 279 (Na-O-Ti stretching[15]), 428, 645, 675, 769, 884, 1366, 1579 and 1775 $cm^{-1}$. However, various other bands 179, 197, 309 (Na-O-Ti stretching[15]), 373, 413, 471, 598, 705, 922 $cm^{-1}$ from the literature[14a] were not explicitly observed above the fluorescence background. Ti-O-Ti stretching vibrations occur between 500 and 800 $cm^{-1}$ where the differences in the Ti-O bond lengths cause shift of resonance frequencies.[16] The resonance frequency depends on the distance between Ti and O and coordination.[16–17] The interatomic distance between Ti and O is severely influenced by the morphology.[2i] Compare the Ti-O bond lengths in as-prepared $Na_2Ti_3O_7$ nanorods with sodium trititanate in Refs.[13–14] Note that the pure Ti-O-Ti framework for layered titanates has three $A_g$ symmetric modes at around 270, 450, and 700 $cm^{-1}$.[17–18]

In a previous investigation it is noted that the vacancy sites (□) of layered $H_{0.7}Ti_{1.825}□_{0.175}O_4{\cdot}H_2O$ depict Lewis acidity.[2i] Essentially, the co-ordinately unsaturated $Ti^{4+}$ and -OH group act as Lewis and Brønsted acid sites, respectively. On titanate nanostructure a number of -OH groups with different acid strengths can be identified. The Brønsted acidity does not differ between $H_2Ti_3O_7$ and $H_{0.7}Ti_{1.825}□_{0.175}O_4{\cdot}H_2O$ nanosheets despite the latter contained a large number of defect sites than the former.[2i] By given the fact that the present nanostructure is a combination of titanate nanotubes and nanosheets a large density of defects is expected. Furthermore, the curvature of nanotube induces the Brønsted acidity, not the composition of the titanate material.[2i,7e,12] The Brønsted acid strength of the -OH bridging groups is higher than the terminal -OH groups. Interestingly, the two types of -OH bridging groups (internal or external) are not very different in the Brønsted acid strengths. On the other hand, in the case of $TiO_2$ (Ref.[19]) an increase of $Ti^{3+}$ is noted after UV treatment ($TiO_2$ or Ti-O were reduced to $Ti^{3+}$). In conjunction with the above discussion, the observed changes in the Raman spectrum due to UV-Vis treatment can be understood. Depending on the illumination energy, electron is excited from the valence band (VB) to a higher excited state in the conduction band (CB). This hot electron relaxes to the bottom of the CB via $e^-/e^-$ and or $e^-$/phonon scattering depending on the excess energy. We will see that the conductivity of our titanate sample is not significantly high and hence, $e^-$/phonon scattering may be a relaxation mechanism. Please note that we have no evidence to confirm the scattering mechanism to be $e^-$/phonon. The hole in the VB captures the $e^-$ from the surface adsorbents, for instance $O_2^-$. After UV-Vis treatment, on the overall scenario, the bands above 420 $cm^{-1}$ have shown increased intensity. Notably, the band corresponding to Na-O-Ti stretching (279 $cm^{-1}$) did not show any shift due to UV-Vis treatment. It means that either there are no chemisorbed species or if present, they cannot be driven away in ambient via UV-Vis treatment. In contrast, after UV-Vis treatment the bands centred at ~428 and 884 $cm^{-1}$ were blue shifted ~10 and 7 $cm^{-1}$, respectively which correspond to Ti-O-Ti stretching vibrations. This blue shift can be attributed to reduction of Ti-O to $Ti^{3+}$ which has higher bond strength/spring constant.[19] The extent of delocalization of electron density on the Ti—O—Ti bond is more in the nanotubes than that of nanosheets.[20] A combination of the nanotubes and nanosheets enables a spatially anisotropic delocalization of electron density which may help to enhance the chemisorption phenomenon. Furthermore, the bands centred at 645, 675, 1366 and 1579 $cm^{-1}$ were better resolved after UV-Vis treatment. Employing confocal Raman spectroscopy to detect the effect of UV-Vis treatment enhances the understanding of the surface properties at or sub surface of the titanate-like proton exchange semiconductors. XRD pattern and Raman spectrum of the titanate nanosheets are closely comparable to that of titanate bulk material which suggests a strong similarity between the crystal structures.

Survey and core-level (N1s, C1s and Cl2p) spectra from PANI are shown in Figure 3. Survey spectrum evidenced C, O, N and Cl where the atomic percentages are 67.2, 18.5, 9.7 and 4.6, respectively. By given the chemical composition of HCl doped PANI, the presence of C, N, Cl is obvious, except O. The presence of oxygen will be discussed later in this section. N1s spectrum is deconvoluted into three peaks with binding energies centred at 399.06, 399.62 and 400.73 eV which were assigned to -N=, -NH- and -$N^+$-, respectively.[21] By considering

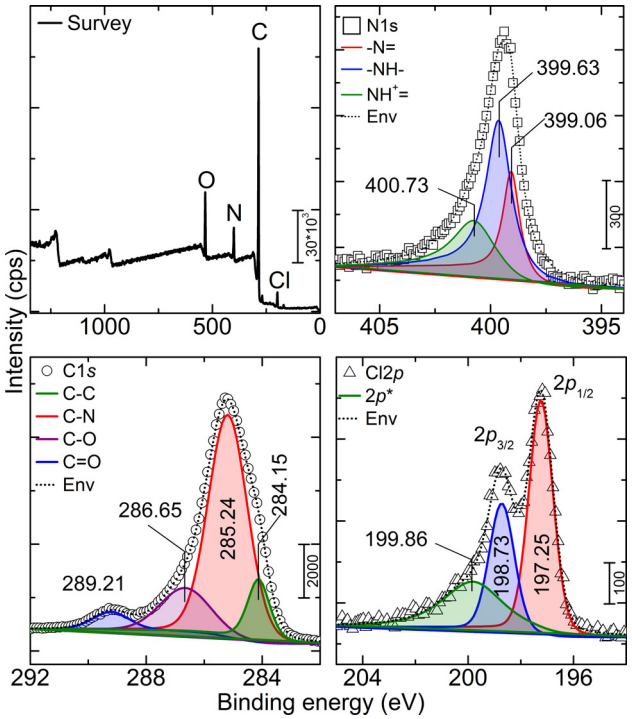


**Figure 3.** Survey and core-level spectra (N1s, C1s, Cl2p) from PANI. The spectral positions (in eV) are annotated on the core-level spectra.

the area under each peak the doping level of PANI is ($-N^+$ -/$N_{total}$) is estimated to be ~26%. This doping percentage is consistent with our ealier observation, where it is elucidated that PANI consists of emeraldine base and salt phases (EB and ES, respectively).[4a] C1s spectrum depicted four distinct components where the contribution at 284.15, 285.24, 286.65 and 289.21 eV were assigned to C=C, C-N, C-$N^+$ or C=$N^+$ and O-C=O groups, respectively.[21a] Notably that the electronegativity of the N is lower than that of O atom which is in line with the increasing binding energy. The doping level or atomic percentage of C-$N^+$ or C=$N^+$ groups are ~25% which is consistent with the evaluation from N1s spectrum. The oxygeneous groups appear due to the oxidation of C, forming C-O, C=O during the synthesis of PANI in addition to chemisorbed oxygen species. Cl2p has shown spin orbit splitting in addition to a low energy peak at 199.86 eV. The doublet can be due to the protonation of PANI by HCl. While the low energy peak cannot be attributed to any specific ionic state which can be due to multiple origins such as by-product formation. In the context of deconvolution of XP spectra,[22] one should note the energy resolution of XPS is determined by the line-width of the excitation (AlKα, 1486.6 eV), inelastic background, resolution of the spectrometer, thermal broadening, life time of the hole, apart from other effects due to approximation(s).[23]

VB spectrum from $Na_{2-x}H_xTi_2O_4(OH)_2$ is shown in Figure 4. The VB edge is determined to be at 2.45 eV below Fermi energy $E_F$. In titanates, a major contribution of O2*p* (*h*-O2*p*) and Ti3d partial density of states (DOS) is expected to the VB and CB, respectively. *h*-O2p indicate hybridized 2p states by given the presence of Ti-O-Na bonds. Notably a minor contribution from Ti3d and O2p orbitals is not denied to the VB and CB, respectively. The peak positions of O2s, Na2p and Ti3p were annotated on the image and the presence of these bands at relatively higher binding energy suggests a well formed crystal structure. A clear signature of Na2p confirms its presence and contribution to deeper VB. A small though distinguishable shoulder at 34.60 eV is noticed. The origin of such shoulders and any contribution of Na2p to CB region may be acquired from density functional theory simulations and inverse photoemission studies.

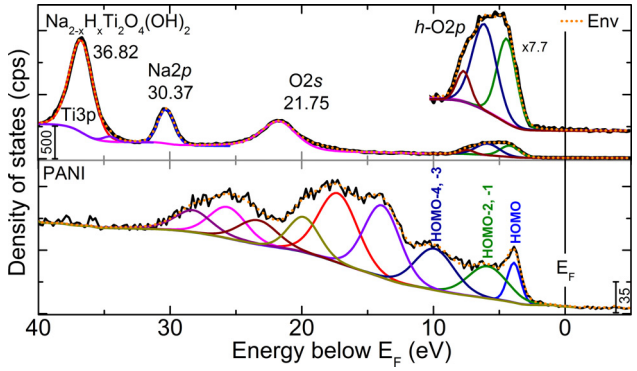


**Figure 4.** VB spectrum from $Na_{2-x}H_xTi_2O_4(OH)_2$ and highly occupied molecular orbitals of PANI. Magnified region on the top part shows hybridized oxygen 2p orbitals (*h*-O2p). Spectral positions are annotated in eV.

In the case of organic semiconductors, molecular orbital picture is more appropriate to describe the occupied states where a major contribution from C and N atoms is expected. Highly occupied molecular orbital (HOMO) and deeper HOMO states (HOMO-1 to HOMO-4) of PANI are shown in Figure 4. HOMO band edge is determined to be at 2.54 eV below $E_F$ and various hybridized density of states extend until ~32 eV. Overlapping features such as HOMO-2, -1 and HOMO-4, -3 are identified on the spectrum. The conductivity of the PANI is determined by the degree of planarity of the aromatic rings. The planarity shifts the molecular orbitals towards $E_F$ which also increases the density of state in its vicinity. This scenario may be expected in relatively thinner films. Conversely, non-planar PANI rings depict relatively lower conductivity (thicker films) and lower density of states near $E_F$, such as the present. As discussed in our previous study the presence of EB, ES and 25% doping confirms the lower density of states near $E_F$.

To detect the presence of intrinsic (radiative) defect states, PL studies were performed on titanate sample with different illumination wavelengths ($\lambda_{ex1-6}$ = 325, 330, 350, 397, 450 and 540 nm), see Figure 5a. The PL spectrum from similar nano-

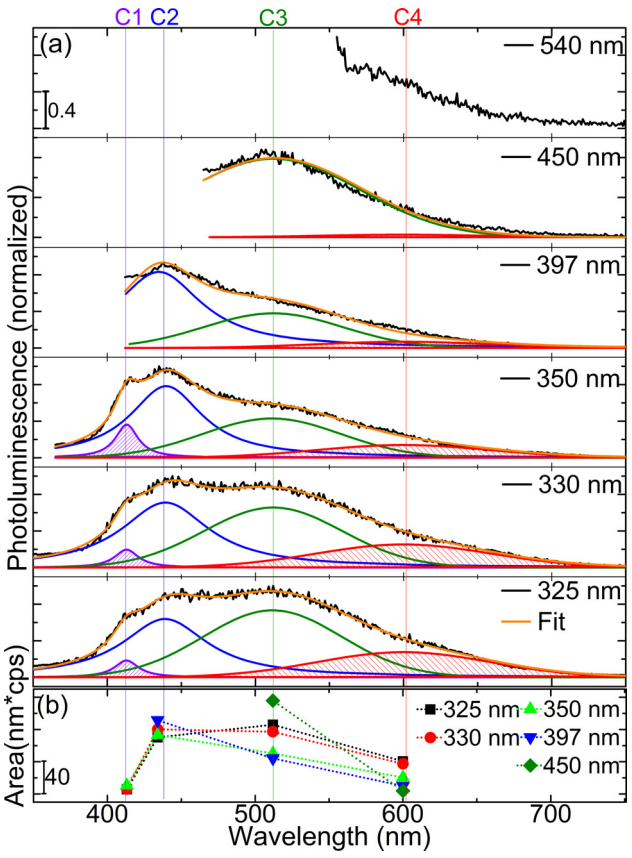


**Figure 5.** (a) Normalized PL spectra from the titanate nanostructure, and (b) area under the peak for various excitation energies, where the connecting lines are for guidance to the eye.

structures was reported earlier however not extensively discussed.[3a] The first three ($\lambda_{ex1}$ through $\lambda_{ex3}$) wavelengths correspond to super-gap excitations and the latter three ($\lambda_{ex4}$ through $\lambda_{ex6}$) were chosen to be less than that of band gap energy of titanate. The PL spectra were deconvoluted (starting with spectrum from $\lambda_{ex5}$) into 2–4 peaks (C1, C2, C3 and C4) depending on the excitation wavelength. As they evolve, in the deconvolution, the centre wavelength and its width were fixed and area is allowed to vary. C1, C2, C3 and C4 were positioned at 418, 438, 517 and 612 nm, respectively and the corresponding area under the each of the peaks is shown in Figure 5b. For illuminations $\lambda_{ex1}$, $\lambda_{ex2}$ and $\lambda_{ex3}$ the intensity changes for all four bands can be compared. While for $\lambda_{ex4}$ and $\lambda_{ex5}$ illuminations, area under the C3 and C4 can be compared.

The broad visible emission is primarily related to self trapped excitons and/or oxygen related defects in the titanate nanostructures nevertheless, the origin of each component is discussed in the following. The C1 is ascribed to self trapped excitons located at octahedra ($TiO_6$), while C2 and C3 are ascribed to oxygen vacancy ($V_O$) defects. C2 is originated from shallow trap state and assigned to $Ti^{+3}$ just below the CB. A clear distinction is seen between the emission lines C1 and C2, which are energetically closer when compared to the other bands. The emission band at C4 might be assigned to electron transition from the $F^+$ centre to the acceptor level just above the VB.[24] The three above band gap excitation $\lambda_{ex1}$, $\lambda_{ex2}$ and $\lambda_{ex3}$ have resulted in similar spectral features and the intensity changes in the all bands can be compared.

In the context of super-gap illuminations, hot electrons relax to the bottom of the CB before radiatively recombine with a hole in the VB. C1 appeared to be relatively sharp peak and the population of which increases as the illumination energy decreases. The intensity of C2 varied with decreasing illumination energy. Such a variation is more explicit for C3 and C4 cases where the intensity decreased with decreasing illumination energy. The three sub band gap excitations $\lambda_{ex4}$, $\lambda_{ex5}$ and $\lambda_{ex6}$ have resulted in distinct spectral features. For an illumination at 397 nm C2, C3 and C4 bands are seen. For 450 nm illumination C3 and C4 are visible where the intensities of these bands are found to be the highest and the lowest, respectively. Interestingly for $\lambda_{ex6}$ illumination we can still see some part of C4 emission, however, this peak is clear at 450 nm excitation. The relaxation time of hot carrier in the CB depends on the illumination energy. Once the hot charge carriers are relaxed the radiative and non-radiative transitions take place. PL is a measure of radiative transitions which is balanced against trapping/non-radiative transitions. Hence the intensity changes ($\lambda_{ex1}$ to $\lambda_{ex3}$) to the various bands can be attributed to such a balance. Also one needs to consider the excitation volume (wavelength dependent) to distinguish the surface bound radiative defects. Further studies on carrier dynamics are warranted to distinguish the various factors.

Composite devices (ITO/titanate-PANI/ITO) and devices with individual components, *viz* ITO/titanate/ITO and ITO/PANI/ITO were investigated. *IV*-characteristics of the pure PANI (Ref.[4a]) and titanate-PANI devices under dark and UV-Vis illumination are shown in Figure 6a and b, respectively. Also, the *IV*-spectra

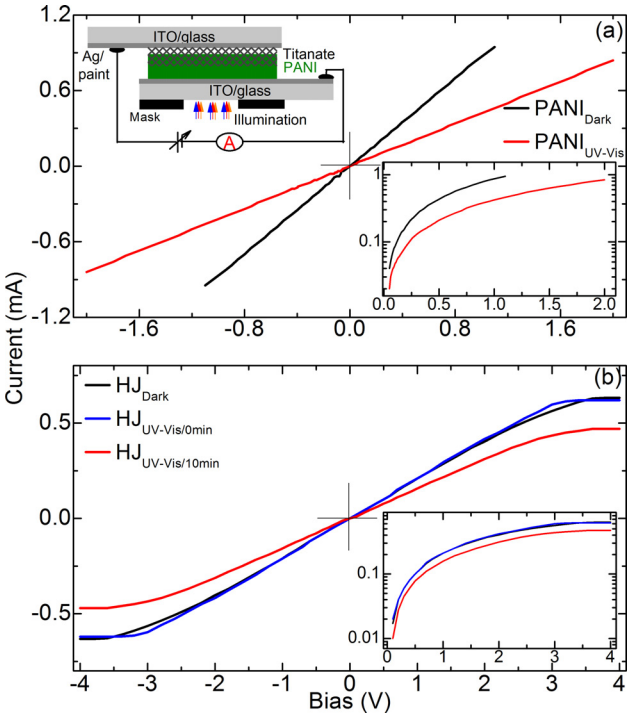


**Figure 6.** Photoresponse of the (a) PANI (Ref.[4a]), and (b) titanate-PANI devices. Inserts show device structure and *IV*-spectra on semi-log scale.

are shown on semi-log scale as corresponding inserts. It is notable that ITO/titanate/ITO device has shown relatively high resistance (> 200 MΩ) in both dark and illuminated condition. In this case, by given the device configuration and the limitation of our ammeter (Figure 6a, insert) we were not able to deduce the *IV*-response. However, in the context of composite devices, PANI impregnates the titanate microstructure and decreased the overall resistance of the device.

The *IV*-response[4a] from PANI is shown in Figure 6a, where a negative PR is observed. Our earlier study indicated the presence of mixed EB and ES in PANI, where EB is in relatively higher fraction than the ES phase.[4a] Such mixed state PANI would perhaps depict polaron (single and or bipolaron) and exciton-dominated dynamics in EB and ES regions, respectively. Hence under dark condition polarons or bipolarons enable the conductivity of PANI where quasi 1D and 3D variable range hopping models are applicable.[25] Under visible (green) illumination (a) the charge carriers generated in ES/ leucoemeraldine base (LEB) interface are trapped at LEB regions where the latter are transparent to green light.[26] Additionally, equal fractions of LEB and pernigraniline base can be present.[26] Furthermore, photo-oxidation transforms ES (already polaronic) into pernigranil salt which is not a good conductor and hence decreases the conductivity or increases the resistance of the device.[27]

In the context of titanate-PANI devices the multiple interfaces between the constituting materials classify these devices into a 'nanocomposite' category. However, the microscale integrity of the titanate nanostructure is preserved. In this case an ensemble effect is reflected in the *IV*-characteristics.

Under dark condition a measurable resistance (within our instrumentation limits) is noted. The complex nanoarchitecture can be reduced to a single resistance model in which PANI and titanate are connected in parallel.

The resistance values (for similar device dimensions) differ nearly 50 times. Hence the majority of the electrical conduction in dark takes place via PANI. Under illumination, in the case of pure PANI an increase in the resistance is noted due to carrier trapping. In titanate nanostructure, upon suitable illumination electron hole pairs are generated. After hot carrier relaxation the electrons and holes may be dissociated into free carriers depending on the interfacial dynamics. In the case of PANI, under illumination excitons are created which then dissociate (as we note a change in the conductivity). Then the free holes and electrons migrate to the corresponding electrodes. Although we are not certain to determine the conductivity contribution of titanate to the total structure, the nano-architecture of titanate enormously increases the interface of the titatane-PANI, which may offer relatively more sites for exciton disassociation. We calculated the resistance (linear fits, not shown) of each of the devices and define a percentage change as following. $\triangle R/R = (R_{UV\text{-}Vis} - R_{dark}) / R_{dark}) \times 100\,\%$, where R stands for resistance of the device. By using this definition, $\triangle R/R$ is calculated yielding ~111% and ~31% from PANI and titanate-PANI devices, respectively. The $\triangle R/R$ from PANI device is ~80% higher than that of titanate-PANI. In the presence of titanate the composite device has shown reduced negative photoresponse. This reduction is explained in the following. The carrier trapping effectively decreased in the presence of titanate nanostructure. As mentioned earlier PANI consists of EB and ES regions which are now distributed across titanate nanostructure. Hence the photogenerated charges are effectively collected at titanate interface before being trapped. Despite, it might also be the case that the titanate is simply separating the EB and ES regions than collecting the charge carriers, which of course depends on the band alignment. Since it is still a negative photoresponse, the contribution from PANI is predominant. Notably, the photoresponse of titanate-PANI is on minutes time scale (see Figure 6b), which might be associated with charge carrier traps and perhaps desorption of oxygen related functional groups from titanate under UV-Vis illumination (see the discussion on Raman spectra). In our earlier report[4a] we have shown that by decreasing the density of EB regions the polarity of the photoresponse can be controlled. Here we show that if EB and ES regions are effectively separated the photogenerated charge carriers can be collected efficiently which decreases the negative PR.

## Conclusions

Integrated structure of titanate nanotubes and nanosheets is evidenced from HR-TEM and SEM micrographs. Various diffraction planes were identified in the XRD pattern and lattice parameters indicated an orthorhombic lattice, where the interlayer distance is higher than pure layered type titanates. Raman spectra before and after UV-Vis treatment revealed surface bound chemisorbed oxygeneous groups due to the presence of defects. Importantly, Na—O—Ti stretching did not depict any changes to its Raman frequency, in contrast to Ti-O-Ti. XPS survey and core-level analyses revealed the doping density of PANI to be ~25% with contributions of -N=, -NH- and $-N^+-$ groups. HOMO and VB were also investigated and the corresponding band edges were found to be at 2.54 and 2.45 eV below $E_F$ for PANI and titanate samples, respectively. PL at different illumination energies revealed the presence of oxygen vacancy related defects and their varying occupancies. The negative photoresponse of nanocomposite device is nearly 4 times lower than that of pure PANI. The nanoscale architecture of the titanate sample enables an effective separation of EB and ES regions of PANI channelizing the charge carriers. The slow photoresponse of the titanate-PANI device may have multiple origins such as carrier traps under illumination and mobility related effects.

## Acknowledgements

S.V. and V.J.B thank TUBITAK (TUBITAK-BIDEB 2221-Fellowships for Visiting Scientists and Scientists on Sabbatical) for the postdoctoral fellowship. Y.E. thanks TUBITAK-BIDEB for a PhD scholarship. T.U. thanks The Turkish Academy of Sciences - Outstanding Young Scientists Award Program (TUBA-GEBIP) for partial funding.

**Keywords:** heterojunction · photoresponse · valence band · core-level XPS · HOMO

[1] H. Izawa, S. Kikkawa, M. Koizumi, *J. Solid. State Chem.* **1985**, *60*, 264–267.
[2] a) D. V. Bavykin, J. M. Friedrich, F. C. Walsh *Adv.Mater.* **2006**, *18*, 2807–2824; b) S. K. Parayil, A. Razzaq, S.-M. Park, H. R. Kim, C. A. Grimes, S. I. In, *Appl. Catal. A.* **2015**, *498*, 205–213; c) Y. Ishikawa, S. Tsukimoto, K. S. Nakayama, N. Asao, *Nano Lett.* **2015**, *15*, 2980–2984; d) M. C. Runkel, O. Wittich, A. Feldhoff, M. Wark, T. Bredow, *J. Phys. Chem. C.* **2015**, *119*, 5048–5054; e) K. Okada, G. Asakura, Y. Tokudome, A. Nakahira, M. Takahashi, *Chem. Mater.* **2015**, *27*, 1885–1891; f) X. G. Xu, X. Ding, Q. Chen, L.-M. Peng, *Phys. Rev. B.* **2007**, *75*, 035423; g) A. S. Nair, Z. Peining, V. J. Babu, Y. Shengyuan, P. Shengjie, S. Ramakrishna, *RSC Adv.* **2012**, *2*, 992–998; h) H. Zhang, G. R. Li, L. P. An, T. Y. Yan, X. P. Gao, H. Y. Zhu, *J.Phys.Chem.C.* **2007**, *111*, 6143–6148; i) M. Kitano, E. Wada, K. Nakajima, S. Hayashi, S. Miyazaki, H. Kobayashi, M. Hara, *Chem. Mater.* **2013**, *25*, 385–393; j) S. Cravanzola, L. Muscuso, F. Cesano, G. Agostini, A. Damin, D. Scarano, A. Zecchina, *Langmuir.* **2015**, *31*, 5469–5478.
[3] a) V. J. Babu, S. Vempati, S. Ramakrishna, *RSC Adv.* **2014**, *4*, 27979–27987; b) P. H. Gonzalez, M. Pedroni, F. Piccinelli, L. L. Martin, S. Polizzi, M. Giarola, G. Mariotto, A. Speghini, M. Bettinelli, I. R. Martin, *J. Lumin.* **2011**, *131*, 2473–2477.
[4] a) S. Vempati, S. Ozcan, T. Uyar, *Appl.Phys.Lett.* **2015**, *106*, 051106; b) R. P. McCall, J. M. Ginder, M. G. Roe, G. E. Asturias, E. M. Scherr, A. G. MacDiarmid, A. J. Epstein, *Phys. Rev. B.* **1989**, *39*, 10174–10178; c) J. Stejskal, R. G. Gilbert, *Pure Appl. Chem.* **2002**, *74*, 857–867.
[5] Z.-R. Tang, X. Yin, Y. Zhang, Y.-J. Xu, *Inorg.Chem.* **2013**, *52*, 11758–11766.
[6] a) Q. Chen, G. H. Du, S. Zhang, L.-M. Peng, *Acta Crystalogr B.* **2002**, *58*, 587–593; b) X. Sun, Y. Li, *Chem. Eur. J.* **2003**, *9*, 2229–2238; c) D. V. Bavkin, A. A. Lapkin, P. K. Plucinski, J. M. Friedrich, F. C. Walsh, *J. Phys. Chem. B.* **2005**, *109*, 19422—19427.
[7] a) T. P. Feist, P. K. Davies, *J.Solid State Chem.* **1992**, *101*, 275–295; b) H. Y. Zhu, Y. Lan, X. P. Gao, S. P. Ringer, Z. F. Zheng, D. Y. Song, J. C. Zhao, *J.Am.Chem.Soc.* **2005**, *127*, 6730–6736; c) K. Kiatkittipong, C. Ye, J. Scott, R. Amal, *Cryst.Growth Des.* **2010**, *10*, 3618–3625; d) J. Huang, Y. Cao, Q. Huang, H. He, Y. Liu, W. Guo, M. Hong, *Cryst.Growth Des.* **2009**, *9*, 3632–3637; e) R. Ma, Y. Bando, T. Sasaki, *Chem.Phys.Lett.* **2003**, *380*, 577–582;

f) J. Yang, Z. Jin, X. Wang, W. Li, J. Zhang, S. Zhang, X. Guo, Z. Zhang, *Dalton Trans.* **2003**, 3898–3901.
[8] E. Morgado, M. A. S. de-Abreu, G. T. Moure, B. A. Marinkovic, P. M. Jardim, A. S. Araujo, *Chem. Mater.* **2007**, *19*, 665–676.
[9] *$TiO_2$ consists of distorted $TiO_6$ octahedral with two longer Ti-O bonds (1.980 Å). The remaining four shorter (1.934 Å) result in Ti-O-Na bonds.*
[10] M. Sugita, M. Tsuji, M. Abe, *Bull.Chem.Soc.Jpn.* **1990**, *63*, 1978–1984.
[11] J. I. Langford, A. J. C. Wilson, *J. Appl. Cryst.* **1978**, 102–113.
[12] Q. Chen, W. Zhou, G. H. Du, L.-M. Peng, *Adv.Mater.* **2002**, *14*, 1208–1211.
[13] Y. V. Kolenko, K. A. Kovnir, A. I. Gavrilov, A. V. Garshev, J. Frantti, O. I. Lebedev, B. R. Churagulov, G. V. Tendeloo, M. Yoshimura, *J. Phys. Chem. B.* **2006**, *110*, 4030–4038.
[14] a) S. Papp, L. Korosi, V. Meynen, P. Cool, E. F. Vansant, I. Dekany, *J. Solid State Chem.* **2005**, *178*, 1614–1619; b) C. E. Bamberger, G. M. Begun, *J. Am. Ceram. Soc.* **1987**, *70*, C48-C51.
[15] Y. Su, M. L. Balmer, B. C. Bunker, *J. Phys. Chem. B.* **2000**, *104*, 8160–8169.
[16] *$H_2Ti_3O_7$ nanosheets: 680 $cm^{-1}$ (three edge-shared $TiO_6$ octahedra that are linked by corner-sharing) $H_{0.7}Ti_{1.825}\square_{0.175}O_4$ $H_2O$ nanosheets: 700 $cm^{-1}$ (infinitely edge-shared $TiO_6$ octahedra) and the difference is attributed to the weaker Ti – O bond strength of the former. □ denote vacancy.*
[17] M. J. Paek, H. W. Ha, T. W. Kim, S. J. Moon, J. O. Baeg, J. H. Choy, S. J. Hwang, *J. Phys. Chem. C.* **2008**, *112*, 15966 – 15972.
[18] a) E. Horvath, A. Kukovecz, Z. Konya, I. Kiricsi, *Chem. Mater.* **2007**, *19*, 927 – 931; b) S. Nosheen, F. Galasso, S. L. Suib, *Langmuir.* **2009**, *25*, 7623 – 7630; c) T. Beuvier, M. Richard-Plouet, L. Brohan, *J. Phys. Chem. C.* **2010**, *114*, 7660 – 7665; d) H. Liu, D. Yang, Z. Zheng, X. Ke, E. Waclawik, H. Zhu, R. L. Frost, *J. Raman Spectrosc.* **2010**, *41*, 1331 – 1337.
[19] S. Saekow, W. Maiakgree, W. Jarernboon, S. Pimanpang, V. Amornkitbamrung, *J. Non-Cryst. Soilds.* **2012**, *358*, 2496–2500.
[20] G. V. Gibbs, D. F. Cox, K. M. Rosso, *J. Phys. Chem. A.* **2004**, *108*, 7643 – 7645.
[21] a) A. V. Naumkin, A.K.-Vass, S. W. Gaarenstroom, C. J. Powell in *NIST X-ray Photoelectron Spectroscopy Database, Vol. NIST Standard Reference Database 20*, Version 4.1 (Ed. Eds.: Editor), U.S. Secretary of Commerce, City, **2012**; b) O. Compton, S. Nguyen, *Small.* **2010**, *6*, 711–723; c) Z. Tong, Y. Yang, J. Wang, J. Zhao, B.-L. Suc, Y. Li, *J. Mater. Chem. A.* **2014**, *2*, 4642.
[22] *The presence of an electronic state may yield a clear or less clear feature in the spectrum however, adding an additional peak to the deconvolution does not necessarily suggest an electronic state unless otherwise proven. Furthermore, if one expects an electronic state at a particular energy, then of course deconvolution can be employed to determine the percentage contribution.*
[23] C. S. Fadley, D. A. Shirley, *J. Res. Nat. Bur. Stand.* **1970**, *74 A*, 543.
[24] B. Santara, P. K. Giri, K. Imakita, M. Fujii, *Nanoscale.* **2013**, *5*, 5476–5488.
[25] a) V. J. Babu, S. Vempati, S. Ramakrishna, *Mater. Sci. Appl.* **2013**, *4*, 1–10; b) V. I. Krinichnyi, *Appl. Phys. Rev.* **2014**, *1*, 021305.
[26] D. M. Bubb, S. M. O'Malley, C. Antonacci, R. Belmont, R. A. McGill, C. Crimi, *Appl. Phys. A.* **2005**, *81*, 119–125.
[27] C. S. Ryoo, E. Y. Jeon, J. H. Kim, J. H. Rhee, H. Lee, *Synth. Met.* **1993**, *55*, 200–205.

Submitted: September 1, 2016
Accepted: October 28, 2016